DESIGN AND EVALUATION OF A TEST PLATFROM FOR THERMAL MECHANICAL AND ACOUSTICAL

LOADING

by

ABDI JASMIN

A thesis submitted in fulfillment of the requirements
for the Honors in the Major Program in Mechanical Engineering
in the College of Engineering and Computer Science
and the Burnett Honors College
at the University of Central Florida
Orlando, Florida

Spring Term, 2015

Thesis Chair: Ali P. Gordon, Ph.D.

Abstract

A test device for thermal, mechanical, and acoustical loading has been designed to replicate the combined extreme environment to which hypersonic fuselage components are exposed. The fuselage panels are typically subjected to super-imposed cycling from hypersonic shock/impingement and aerodynamic pressure from the usual ascent-cruise-decent mission profile of the aircraft combined with mechanical vibration at acoustic frequencies; moreover, these slender components will undergo conventional mechanical fatigue with compressive mean stress due to geometric constraint. A universal column buckling frame, an acoustic horn, and a custom-made quartz-lamp furnace is tuned via a GUI to allow users to design cyclic load profiles that idealize the thermo-acousto-mechanical loading of critical panels.

Acknowledgement

I would like to express the deepest appreciation to my committee chair Dr. Ali Gordon, who has showed the attitude and the substance of a genius: he continually and persuasively conveyed a spirit of adventure in regard to research and scholarship, and an excitement in regard to mentoring. Without his supervision and constant help this dissertation would not have been possible.

I would like to thank my committee members, Dr. Kuo-Chi 'Kurt' Lin and Dr. Necati Catbas for their support. In addition, a thank you to the Brunet Honors College for their financial support granted through the Honor in the Major Scholarship.

Table of Contents

Abstract ii
Acknowledgement iii
Table of Contents iv
List of Figures vi
List of Tables vii
Nomenclature viii
Chapter 1. Introduction 1
  Motivation 1
  Overview 2
Chapter 2. Background 4
  Eulerian Buckling 4
  Column Buckling Experiments 9
  Post Buckling Response 11
Chapter 3. Experimental Approach 13
  Test Requirements 13
  Test device Design 14
  Device Performance 19
    Mechanical 19
    Thermal 22
    Acoustical 22
  Test Material 24
  Mechanical Model 25
Chapter 4. Results 27
  Mechanical 27
  Thermal ..... **Error! Bookmark not defined.**
  Acoustical ..... **Error! Bookmark not defined.**
  Combined 27
Chapter 5. Numerical Simulations 28
  Specimen Model 28

Finite Element Model 29
Results 31
Chapter 6. Comparisons and Observations 33
Chapter 7. Conclusion 33
References 34

List of Figures

Figure 1 Critical panels of the DARPA Falcon HTV-3X designed for Mach 5.2. 1
Figure 2 Graphical user interface developed in LabView 3
Figure 3 Stout vs slender component under compressive force P 4
Figure 4 Slender column under bi-clamped boundary condition. 5
Figure 5 Bi-clamped simulation of AISA 304 beam E=27.5e6 psi with dimensions L=0.4m, b=25.4mm, a=2.29mm, P=1.3KN. 8
Figure 6 the effect of eccentricity on critical buckling load 9
Figure 7 - Post buckling deformation response of steel. 12
Figure 8 – Bi-clamped testing condition of a 0.41m long specimen. 13
Figure 9 Reconfiguration of the Sanderson frame 14
Figure 10 Load Cell Calibration 15
Figure 11 Furnace triangular design 16
Figure 12 Thermocouple settings for temperature profile and PID control. 17
Figure 13 Horn assembly on 8020 frame 17
Figure 14 Accelerometers on sample 18
Figure 15 Platform for Combine Extreme Environments (P-CEEn): (a) numerical model and (b) physical device with test specimen 19
Figure 16 Initial load- and displacement-controlled deformation response of specimen A2 20
Figure 17 Cycle load P_{max}=190N, $P_{cr=}$1014N, L=0.4572 21
Figure 18 8 consecutive and consistent cycles 21
Figure 19 Furnace performance 22
Figure 20 Acoustic transfer efficiency 23
Figure 21 Specimen used in the initial phase 23
Figure 22 Southwell Plot 26
Figure 23 Software used for simulation 28
Figure 24 Specimen CAD and dimensions 28
Figure 25 Fixed geometry feature 29
Figure 26 Roller/Sider feature 30
Figure 27 Load being applied to the specimen 30
Figure 28 Final FEM model for buckling analysis 30
Figure 29 Buckling analysis of specimen S28 31
Figure 30 Buckling analysis of specimen S30 32
Figure 31 Buckling analysis of specimen S32 33

List of Tables

Table 1 Specimen dimensions and properties 25
Table 2 Buckling analysis simulation 33

Nomenclature

δ_H	=	Horizontal deflection [mm]
δ_V	=	Vertical deflection [mm]
t_c	=	Compressive dwell period [s]
t_{cyc}	=	Cycle time [s]
A	=	Cross-sectional area [mm^2]
f_a	=	Acoustic frequency [Hz or s^{-1}]
I	=	Moment of inertia [mm^4]
P	=	Compressive Load [kN]
E	=	Young's Modulus [GPa]
L	=	Length of specimen [m]
b	=	Specimen width [mm]
a	=	Specimen thickness [mm]
SPL	=	Acoustic Pressure [dB]
ΔT	=	Temperature Range [°C]
T	=	Temperature [°C]
t	=	time [s]

Chapter 1. Introduction

Motivation

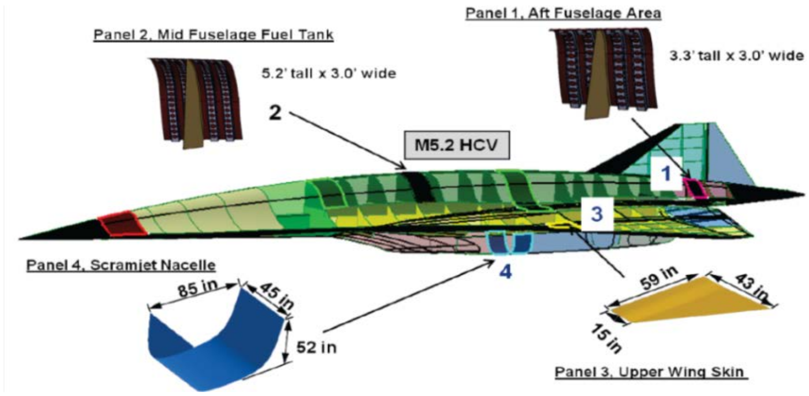

Figure 1 Critical panels of the DARPA Falcon HTV-3X designed for Mach 5.2.

Engineering materials normally do not reach theoretical strength when they are tested in the laboratory. In space-like situations, components and structures are usually subjected to several modes of loading simultaneously. These loads usually affect the strength, deformation, and life of that object or structure in engineering applications. For example, vehicles for aerial combat (e.g. F-22 Raptor, A-10 Thunderbolt II) during operational life will be subjected to various impacts that might result in mechanical damage. An analogous land-based combined extreme environment case would be railroad wheels under thermo-mechanical loading. Railroad wheels experience thermal loading during brake shoe applications. Hot spots develop on the tread of the wheel as it passes under the brake shoe. Thermal stresses on the hot spots are higher than the surrounding cooler material. Oxide formation at the tread (hot spots) and flange regions may be extensive and influence crack nucleation. The hot spots and other critical regions experience many small thermal cycles within major thermal cycles [1]. A test platform capable of replicating the combined extreme environment to which hypersonic fuselage components will be exposed has been developed. In service, (1) thermal cycling load is developed on the components in combination with (2) mechanical vibration at acoustic frequencies due to hypersonic shock/impingements and aerodynamic pressure. Additionally, these relatively thin components will undergo conventional (3) mechanical fatigue with compressive mean stress due to geometric constraints and maneuvers of the vehicle; therefore, the test platform will simulate cycles of thermal, mechanical and acoustic loads superimposed. Having the ability to precisely replicate the working environment of the fuselage components will help to identify life limiting conditions of the materials. It is also an effective method to determine the limits of the structure and make appropriate adjustments when necessary.

Overview

This thesis continues with a review of recent literature relevant to this study in Chapter 2 and a brief background on buckling. Chapter 3 contains information on the experimental approach. Once the test device had been developed, it was paired with a graphical user interface (Fig. 2) developed in LabView. Several experiments were performed in order to calibrate the test device before usage. The strength and the weaknesses of the device were identified and the device was improved as needed.

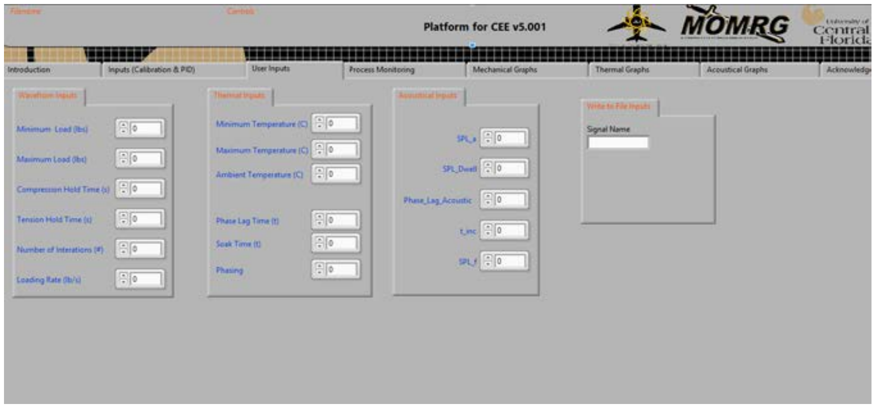

Figure 2 Graphical user interface developed in LabView

Chapter 2. Background

A structural component such as a beam, a column or a rod subjected to a compressional load would normally experience a deformation directly proportional to its length L and the load P and inversely proportional to the young's modulus E of the material. Ideally, a stout enough component will deflect but remain untwisted similar to a coil spring subjected to an axial load and it is not expected to fail (plasticized and flattened) at loads less than the compressive strength of the material. However, if the loaded member is sufficiently slender (the ratio of its length L to its cross-section dimension a is greater than ten), it will deflect and twist and eventually fail under a critical load. This mechanical failure is known as buckling and it is presented in this chapter.

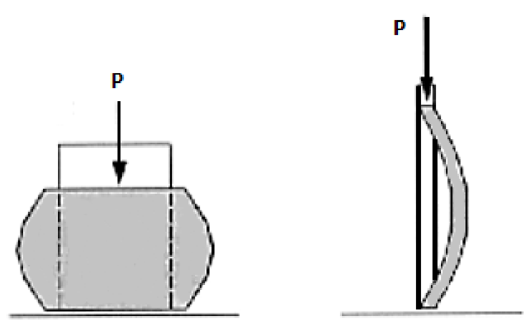

Figure 3 Stout vs slender component under compressive force P

Eulerian Buckling

Buckling, also known as structural instability, is a mechanical failure exhibited by a sufficiently slender column (the ratio of its length L to its cross-section dimension a is greater than ten) under compressive loading, P. It can be classified into two categories: (1) *bifurcation bucking* or (2) *limit load buckling* [2]. Bifurcation buckling occurs when deflection under compressive load goes from axial shortening to lateral deflection. The *critical buckling load* or simply *critical load*, is the load at which the bifurcation occurs. The terms “*primary path*” and “*secondary*” (or “*post buckling path*”) are used to describe the path that exists prior to and after bifurcation buckling. The post buckling path is dependent of structure and loading. In limit load buckling, the structure attains the maximum load without any previous bifurcation [3]. Other classifications of buckling are described with respect to the displacement magnitude or material behavior such as elastic/inelastic buckling.

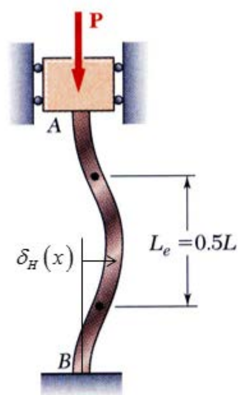

Figure 4 Slender column under bi-clamped boundary condition.

Euler was the first to study elastic stability using the theory of calculus of variations to obtain the equilibrium equation and buckling load of a centrally compressed elastic column. For uniform, perfectly straight, sufficiently slender (the ratio of the length to the cross-section dimensions is greater than 10) and homogenous column as shown in Fig. 1, the theory of bending, first suggested by Bernoulli, represents an accurate approximation to the exact solution according to three-dimensional elasticity [4]. In his work, Euler has assumed that the cross section of the column does not distort during buckling and. With column length, *L*, Young’s Modulus, *E*, and second moment of inertia, I, subjected to an end axial compressive load P, the moment-displacement relation according to the Euler-Bernoulli beam theory is given by

$$M(x) = -EI\frac{d^2\overline{w}(x)}{d\overline{x}^2} \tag{1}$$

Here $\overline{w}(x)$ refers to the transverse displacement, and $\overline{x}$ is the longitudinal coordinate measured from the column base. The cross bar refers to non-linearization by L (e.g. $w = \overline{w}/L, x = \overline{x}/L$). The theory is based on the assumption that plane normal cross-sections of the beam remain plane and normal to the deflected centroidal axis of the beam, and the transverse normal stresses are negligible. Equation (1) provides an essential characteristic of buckling: the failure load depends primarily on the elastic modulus and the cross section stiffness of the material and is almost independent of the material strength or yield limit [4]. In fact, slender columns generally buckle prior to the exceedance of strength or stiffness criteria.

Analysis can be used to develop a deflection model and a critical load for buckling. The general solution of the differential equation is expressed as

$$\delta_H(x) = C_1 \sin\sqrt{\alpha}x + C_2 \cos\sqrt{\alpha}x + C_3 x + C_4 \tag{2}$$

Where α is equal to $\frac{PL^2}{EI}$, and the constants C_1, C_2, C_3 and C_4 are constants of integration. The simplified solution for a bi-clamped case

$$\delta_H(x) = \frac{M}{P}\left(1 - \cos\sqrt{\frac{P}{EI}}\,x\right) \tag{3}$$

Here M in the constant moment developed at the end supports. It can be readily shown that the critical buckling load is:

$$P_{cr} = \frac{4\pi^2 EI}{L^2} \tag{4}$$

Hence, the critical buckling normal stress is given by

$$\sigma_{cr} = \frac{4\pi^2 E}{(L/r)^2} \tag{5}$$

Where $r = \sqrt{I/A}$ is the radius of gyration, and L/r, is the slenderness ratio of column.

These equations are valid only for cases where the deformation can be assumed to be purely elastic in an isothermal environment and under ideal conditions [5]. Figure 5 shows a numerically simulated post buckling response of a slender 304 steel beam under longitudinal compression and the horizontal displacement δ_H in millimeters. The sinusoidal deflection and fixed boundaries predicted by Eq. (3) are verified. A load of 1.3KN was applied to the model and the resulting load factor BLF=1. The buckling load factor (BLF) is the factor of safety against buckling or the ratio of the buckling loads to the applied loads. $BLF=1$ means the applied loads are exactly equal to the estimated critical loads, buckling is expected.

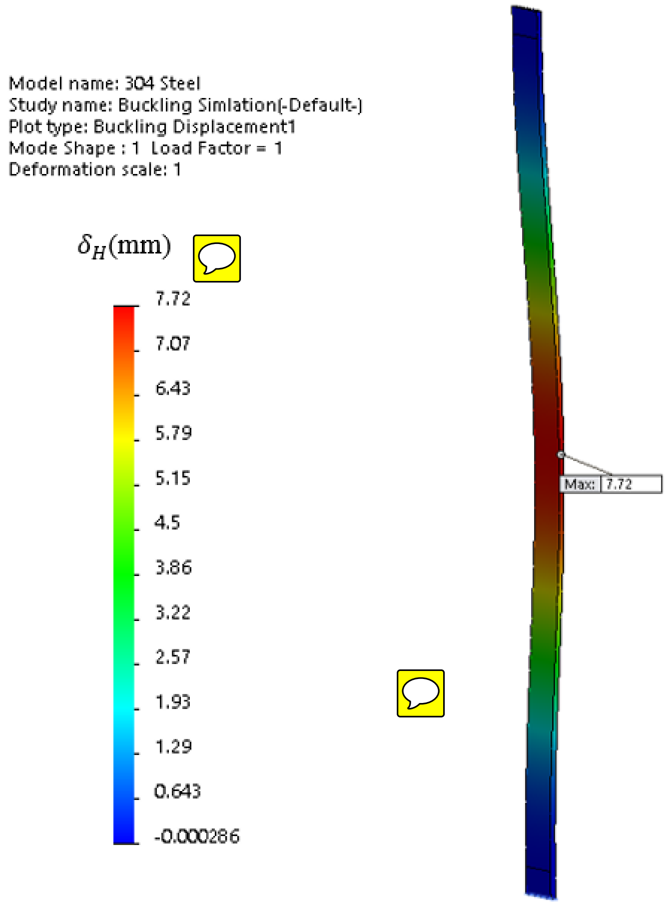

Figure 5 Bi-clamped simulation of AISA 304 beam E=27.5e6 psi with dimensions L=0.4m, b=25.4mm, a=2.29mm, P=1.3KN

Up until now the structural member has been considered to be initially straight and loaded along its neutral axis, but in reality, a structure and its loading will never match these idealizations. That is one reason why materials normally do not reach theoretical strength when they are tested. Small deviations from ideal can be assumed negligible when studying the behavior of structural members such as beams, columns, shafts and rods under tension. However, they can make a difference in determining elastic instabilities. Two types of imperfection that commonly occur when studying buckling 1) load eccentricity, which occurs when the load applied *P* is at a distance *e* from the neutral axis developing a moment $M = eP$ and 2) the presence of an initial deflection δ_0. Figure 6 demonstrates how the critical buckling load will be affected by an increase of eccentricity with respect to the length *L*.

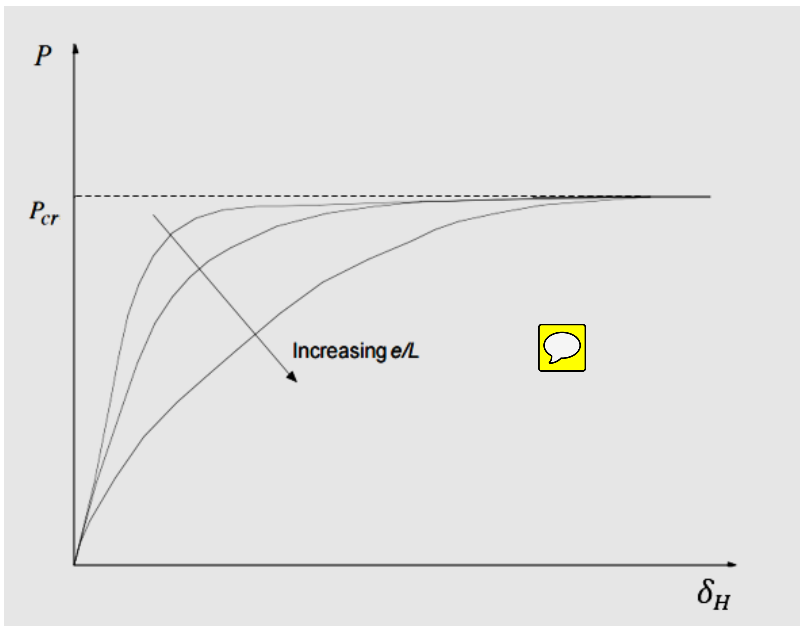

Figure 6 the effect of eccentricity on critical buckling load

Column Buckling Experiments

In an effort to improve effectiveness and accuracy in predicting buckling and post buckling strength, a variety of experiments have been performed. Carpinteri and collegues [6] investigated the dependence of the fundamental frequency on the axial load in slender beams subjected to imposed axial end displacements. Knowing that the presence of an initial curvature (geometrical imperfection) of the beam axis can significantly affect the dynamic structural response of a slender beam, they used equal length specimens with different initial curvatures in hinged–hinged and hinged–clamped conditions. A servo-controlled machine (MTS) with a closed-loop electronic control, having a maximum capacity of 100 kN. In order to apply vibration to the specimen, an electromagnet positioned at mid-height of the tested beam transmitted a sinusoidal force to the beam, controlled in frequency and amplitude by the wave generator. The time history of the beam midpoint transversal displacement, measured with the laser sensor. Data such as (1) axial load with respect to transverse displacement and (2) fundamental frequency versus axial load were generated for analysis. The results were shown for frequencies ranging from 10Hz to 60Hz. They found that a first phase, where the fundamental frequency decreases with the axial load, is followed by a stiffening one, where the trend is reversed. The transition seems to be smoother with geometric imperfection in the specimen.

The behavior of geometrically constrained columns has been studied in high temperature environments [10], and it is well known that under a thermal load, the compressive load in a column will increase due to thermal expansion. Furthermore, Wang indicates that increase in temperature can cause degradation of strength and stiffness properties of a component [7]. Carpinteri confirms the existence of a relationship between the natural frequency and the stiffness of the tested components [6].

Wang [7] investigated the local stability of steel stub columns at elevated temperatures. The experiments consisted of testing 12 stub columns under simultaneous application of load and temperature conditions. The axial load was applied by means of a hydraulic jack and a furnace that generate temperatures up to 1200°C to undertake the fire test. Load versus deflection data were generated at different temperatures and interesting changes in the curves plotted were observed. Data generated from tests indicate that the buckling resistance or ultimate strength of H stub columns decreases with increasing temperature, mainly due to degradation of strength and stiffness properties of steel. Other test devices have been developed to simulate combined load such as torsion and axial compression on similar composite panels [8]; however, no authors have presented research data under conditions where high frequency/low amplitude vibration is combined with compressive buckling at high frequency.

Post Buckling Response

The secondary path or post buckling responses depend on structure and loading. The deformation can be symmetric, asymmetric and may rise or fall below the critical buckling load. Load versus lateral deflection data are traditionally used in post buckling analysis as they are excellent indicators of the buckling event. Alternatively, they do not provide clear information on the energy aspects of the buckling phenomenon as lateral deflection is just perpendicular to the operating load. In a research conducted by Ziółkowski and Imielowski [9], plots of axial load versus axial displacement showing relevant energy information were generated. Axial load versus axial displacement plots show a similar behavior when compared to a typical load versus lateral deflection but the data seems to be a lot smoother and a rounding off of the force curve before actually reaching the Euler load can be clearly noticed. It is a characteristic feature for column-load system imperfections. This can help identify the critical load when live data is being recorded.

Post-buckling response has been investigated for room temperature conditions. For 304 SS slender beam, shown in Fig. 5, the force curve marked with red circles was recorded from an experiment conducted at UCF. The compressive load P was plotted against the transverse deflection δ_H.

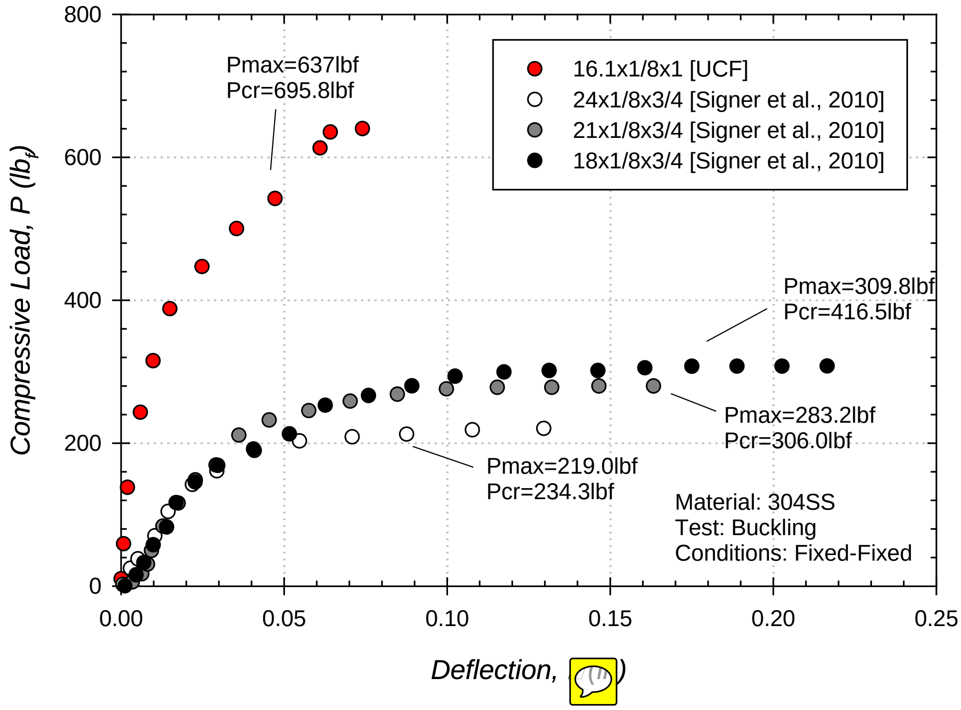

Figure 7 - Post buckling deformation response of steel.

Chapter 3. Experimental Approach

Test Requirements

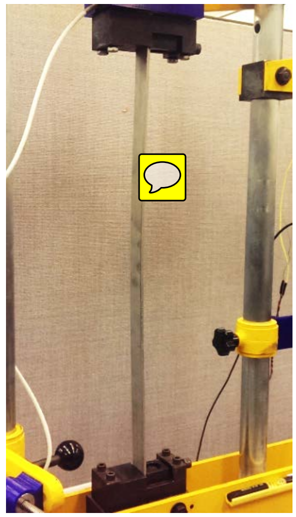

Figure 8 – Bi-clamped testing condition of a 0.41m long specimen.

In order to predict critical bucking in the combined thermo-acousto-mechanical environment, the device must be able to produce accurate buckling response of the specimen used. For this, two sets of experiments will be conducted. The first set of experiments is intended to calibrate and evaluate the performance of the main components of the device, the response of the specimens will be investigated under mechanical cyclic loading (displacement/force control), transverse vibration (250 to 500Hz, 120dB) and thermal cycles (RT to 0.5Tm) separately. For the second set, the full buckling response of the specimens will be investigated and compared with theoretical and simulated data. Lastly, the buckling response of the specimens will be investigated under the combined thermo-acousto-mechanical cycles. The device should be able to provide data for specimens allowed to be elastically deformed to determine the relationship between the cumulative contributions of each load in the elastic deformation range and attempt to use this information to predict the critical load. The loads will be plotted against the displacement history of the midpoint of the specimen which can provide information about the nature of the deformation and the fatigue life of the component. Models of the loads with respect to vertical displacement will also be generated which can provide information on the energy aspects of the buckling phenomenon. Further data analysis will be illustrated later on

Finally, the device will be ready to perform service like test profiles developed using available data history to generate test data that will facilitate the development of mechanical properties utilized in modeling and simulations of the fuselage components.

Test device Design

The developed test platform is composed of three sub-systems: a Sanderson universal manual column buckling test frame, a customized quartz-lamp furnace and an acoustic horn.

Figure 9 Reconfiguration of the Sanderson frame

The Sanderson load frame has been reconfigured (Fig. 7) to allow automated cyclic mechanical loads with the addition of a motor on the lever arm. A translation screw of 1.80 mm per rotation is used to generate the motion of the lever arm. The load frame is equipped with a washer-type load cell (Futek model: LTD 400) positioned at the upper fixed-end boundary of the column specimen to help maintain desired load, a linear displacement transducer (Omega model: LD621-15) on the left side of the load frame that measures the horizontal component of deflection of the specimen, and a second transducer is mounted on the right end of the lever arm to allow the computation of the vertical component of the specimen deflection. The load frame has the ability to accommodate several specimen size from 0.40m to 0.8m, with a 0.05m increment and a thickness of up to 0.004m.

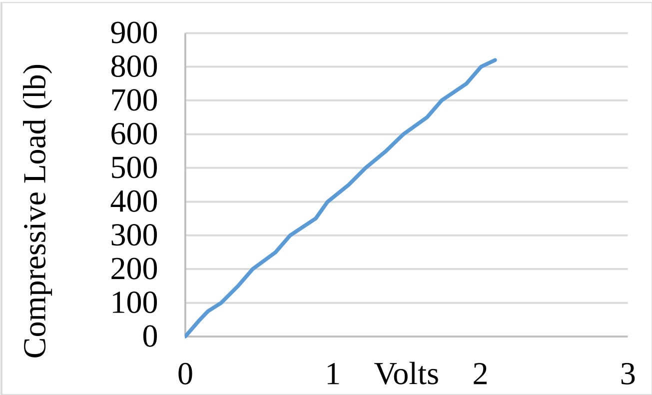

Figure 10 Load Cell Calibration

The compressive load cell was subjected to a known loads between 0kN (0V) and 3.7kN (2.1V). Known displacements between 0 (0V) and 15mm (10V) were prescribed to the spring-loaded, displacement transducer. A high-torque servo-motor was used to drive the power-screw connected to the lever arm. The vertical displacement transducer and the middle plane of the specimen are exactly 0.53m and 0.15m away from the pivot point of the lever arm respectively.

Using similar triangle relationships, the vertical displacement of the specimen is determined from the reading of the vertical transducer. Additional power is supplied to both the load cell, displacement transducer, and the motor via fixed DC power supplies. Input voltage was applied to the motor, and the resulting angular velocity (in rad/s) was determined through a stroboscope. For the motor, an H-bridge circuit combines the fixed power with oscillating signal from the chassis.

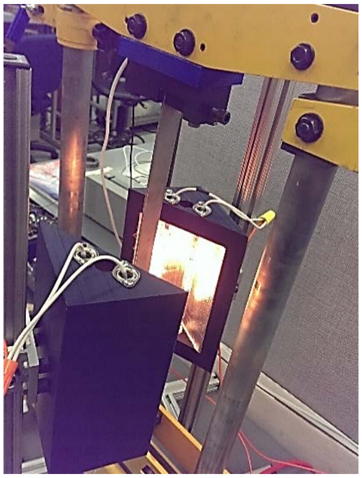

Figure 11 Furnace triangular design

The furnace houses up to a total of six 120V 2000W lamps, four of which are used to provide a uniform heat distribution around the specimen. Behind the lamps, reflective material is attached to the triangular furnace sections to increase the maximum heat potential of the system. Triangular furnace sections were chosen to give a channel for the acoustic system (Fig. 9). The heating elements are controlled by a LabView VI leading to a Watlow PID controller, which sends a control current to a 208V 20A power supply (Research Inc. model: 5620-21-SP34) wired into the four lamp circuit. Five thermocouples attach to the sample at 0%, 33%, 50%, 66%, and 100% length *L* positions in order to get a temperature profile, and the thermocouple placed at 50% is used for PID calculation. All five thermocouples route data back to LabView for recording. The furnace is capable of reaching a maximum temperature of 400°C. For now, a cooling system has not been integrated in the thermal control of the system but it can be integrated in future versions of the device.

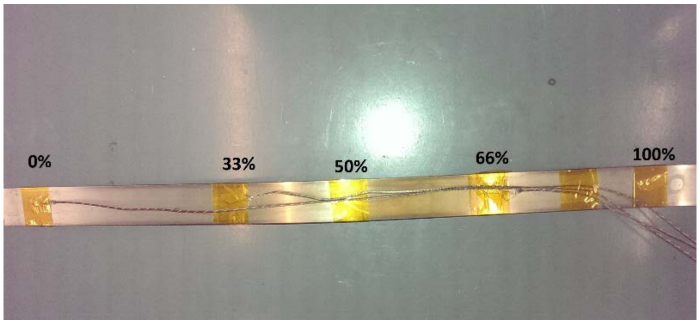

Figure 12 Thermocouple settings for temperature profile and PID control

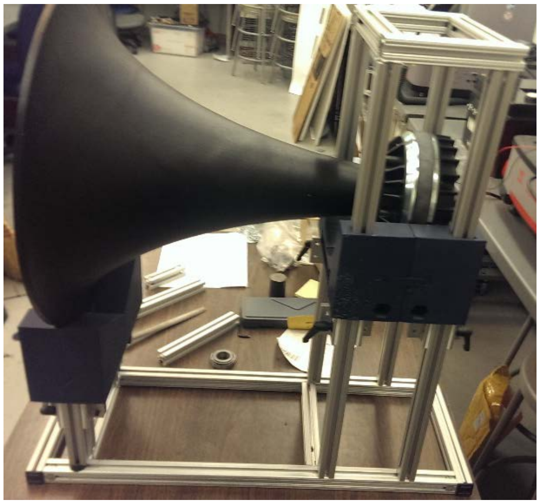

Figure 13 Horn assembly on 8020 frame

The hardware for the acoustic system consists of two ICP accelerometers (Piezotronics model: PCB 352B10), a power amplifier (Russound model: R290DS), a horn driver (BMS model: 4591), and a wave guide (SL Custom 250Hz Tractrix). The driver/horn assembly is mounted with an 8020™ extruded aluminum frame. The frame is made adjustable so that is can be adjusted accordingly to the length of any specimen. An oscillatory voltage waveform (sinusoidal or triangular) of frequency, fa, of 250 or 500Hz and amplitude of 328mV, is output from the NI cDAQ chassis to a 2-channel, dual-source power amplifier (Russound model: R290DS). An 8 or 16Ohm signal is sent to a 2” mid-range, compression driver (BMS model: 4591). A flat front, tractrix-curved waveguide is flush-mounted to the driver. Pre-calibrated (10mV/g), miniature accelerometers (Piezotronics model: PCB 352B10) were attached to the tip of the waveguide and along the length of the sample.

Figure 14 Accelerometers on sample

Device Performance

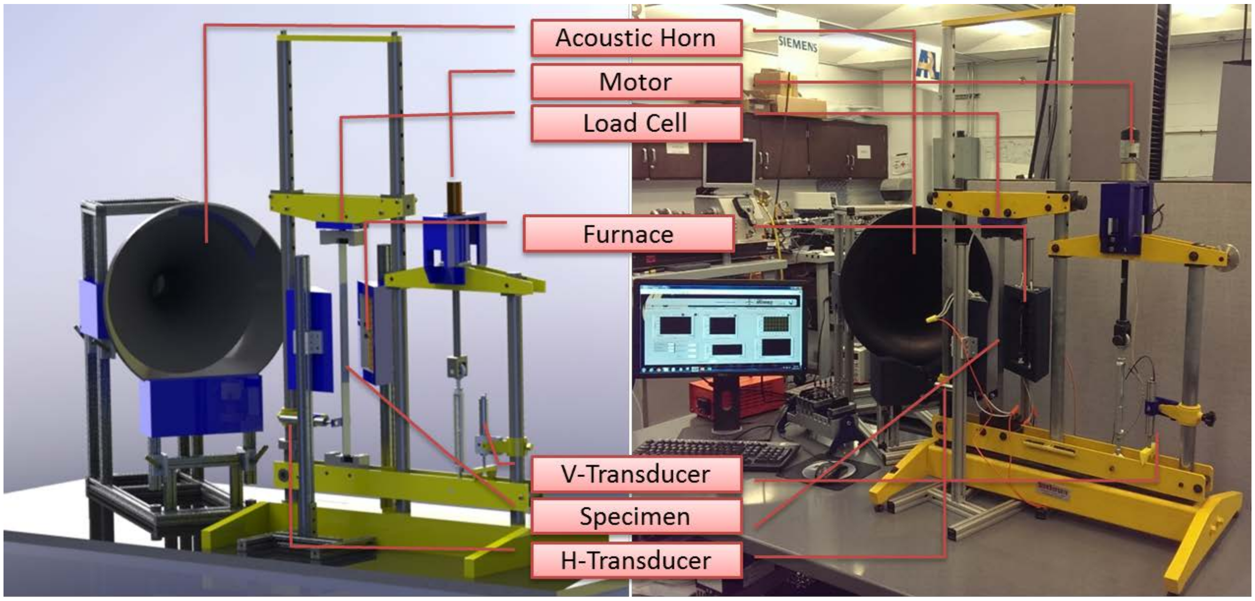

Figure 15 Platform for Combine Extreme Environments (P-CEEn): (a) numerical model and (b) physical device with test specimen

Before conducting any experiments, several calibration experiments were conducted to check validate the performance of the device.

Mechanical

For the initial phase of the mechanical loading experiments, two methods were used to control the load application on the specimen. The first method, load controlled, involves a direct control of a load as high as 333.6 N being applied to the specimen while the vertical and horizontal displacement responses are recorded. The load cycles from a set minimum to a set maximum at a set rate. For the second method, displacement controlled, the specimen was subjected to a range of vertical displacement corresponding to known range of mechanical load at a defined rate while the axial response is recorded. The graph below shows the response of a 0.4m long specimen (Fig. 15) subjected to a loads ranging from 8.9N to 178N at 14N/s. while deforming, the specimen maintained a uniform sinusoidal shape. This data confirms the flexibility of the device when it comes to performing load controlled or displacement controlled experiments.

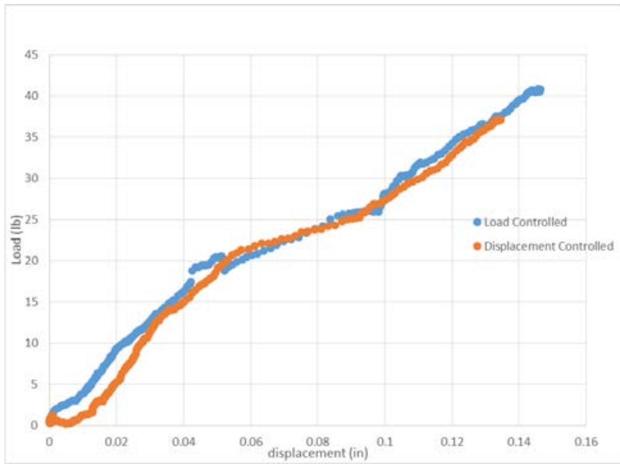

Figure 16 Initial load- and displacement-controlled deformation response of specimen A2

Another important feature of the mechanical component of the device is to be able to apply a mechanical cycling loads to a specimen and record it consistently. For this, a triangular waveform signal was sent to the load control with a maximum load cycle P such that $P \ll P_{cr}$. Load vs time and load vs displacement were recorded and plotted below.

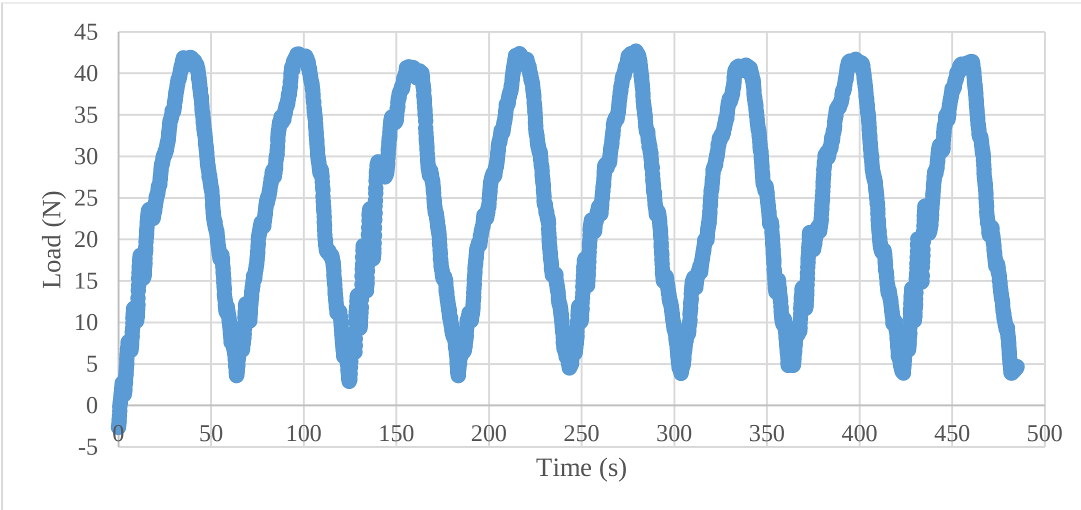

Figure 17 Cycle load P_{max}=190N, P_{cr}=1014N, L=0.4572

The maximum applied load P_{max} (190 N) is only 18.7% of the theoretical critical load (1014 N). The specimen is not expected to deform plastically and this is confirmed in the consistent load vs δ_H response shown in Figure 17.

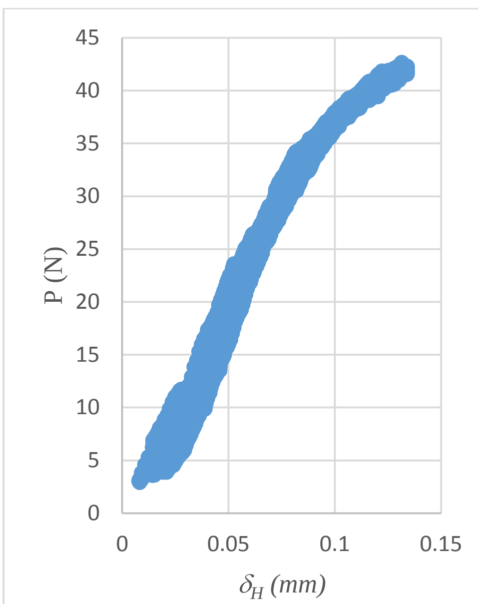

Figure 18 8 consecutive and consistent cycles

Thermal

As stated earlier, the thermal component of the device is only composed of a heating element. The furnace works perfect for isothermal experiments. When it comes to thermal cycling, due to the lack of a cooling system the temperature rises accordingly but does not cool down very fast below the 300°C range. The performance of the furnace is shown below.

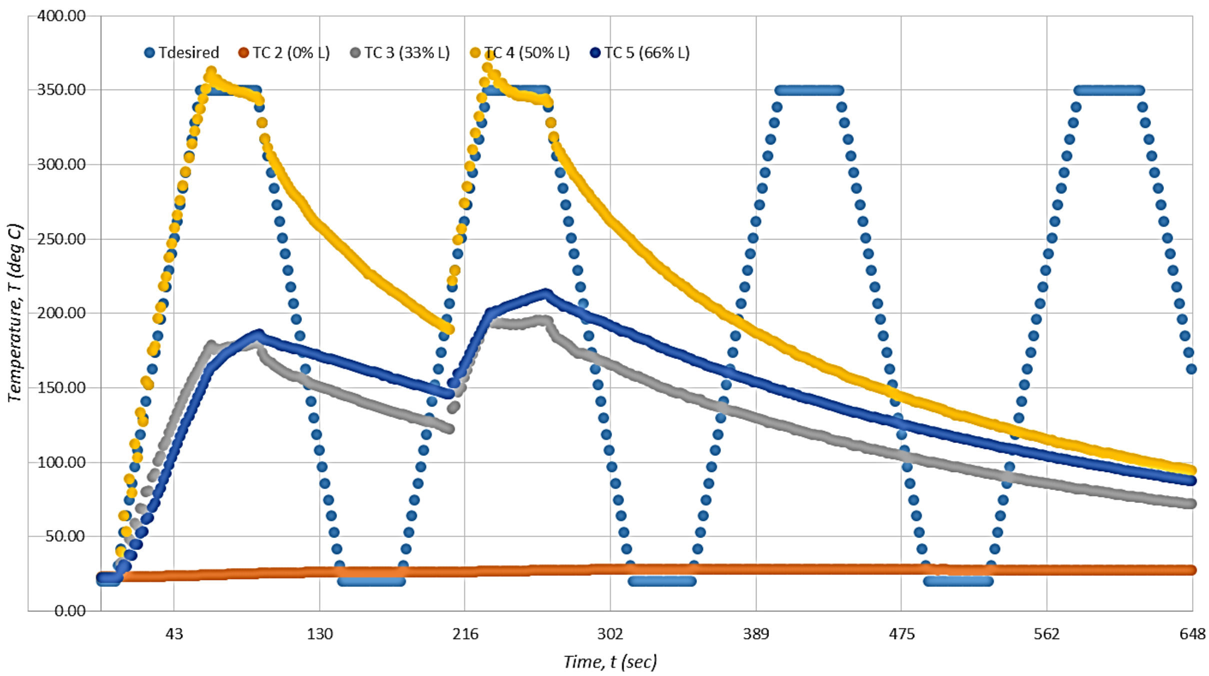

Figure 19 Furnace performance

The data from Figure 19 shows that the temperature profile is not symmetric since the thermocouple reading at the 66% is higher than the reading at 33% due to asymmetric heat flow convection. The thermocouples at 0% and 100% were reading near room temperature.

Acoustical

Thus far, the equipment has performed well at 120dBSPL with both triangular and sinusoidal waveforms, with exceptional performance at 500Hz. Figure 20 shows the acceleration experienced (in gs) at the bottom and mid-point of a test-sample, as well as the acceleration experienced at the mounting fringe of the horn

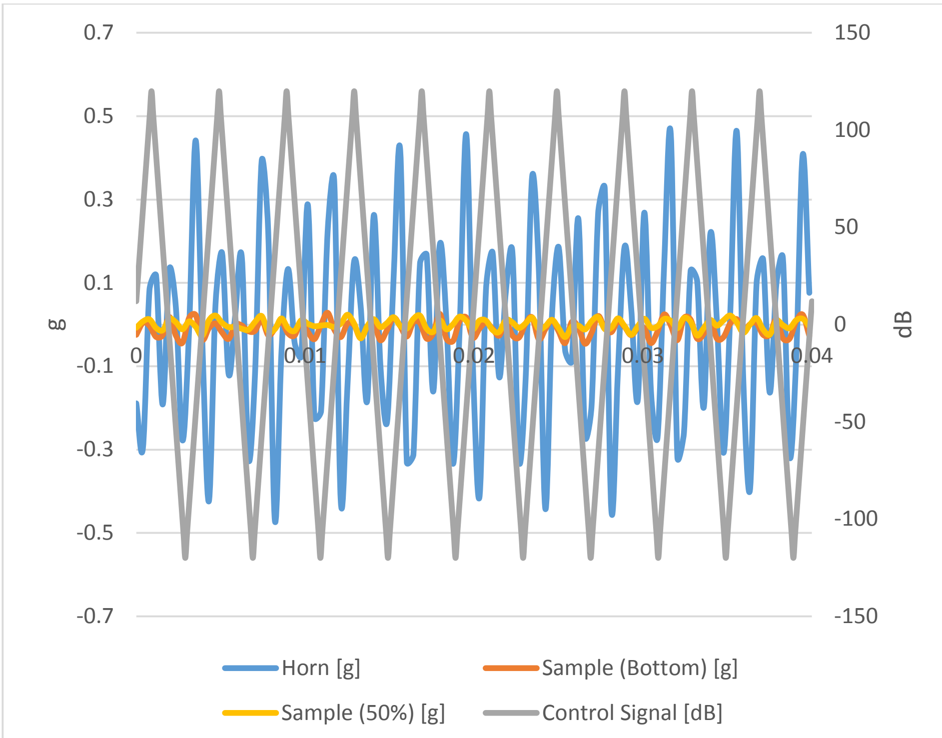

Figure 20 Acoustic transfer efficiency

Figure 21 Specimen used in the initial phase

Test Material

When comparing the elastic buckling behavior of a given structure and that of a geometrically similar model structure not necessarily made of the same material, the Poisson's ratio υ of the materials is usually used as a reference for choice of material for buckling experiments [12]. It has been proven that

$$(P_{cr} / EL^2) = C \tag{6}$$

Where C is a dimensionless number for all similar elastic structures, and

$$(P_{cr} / EL^2) = f(\upsilon) \tag{7}$$

And therefore, for material with equal Poisson's ratio,

$$(P_{cr.1} / P_{cr2}) = (E_1 / E_2)(L_1 / L_2)^2 \tag{8}$$

Several samples of multipurpose 304 stainless steel, having identically uniform cross sections (i.e., a = 3.18mm by b = 25.4mm) but a range of lengths (i.e., between L = 0.4m and 0.8m), were utilized in the test bed development. The specimens are tested in the unpolished condition, and they were incised from hot rolled plate stock (per ASTM A276). At room temperature, elastic modulus, E, is 193GPa, yield strength corresponds, 0.2%YS, to 207MPa, and the coefficient of thermal expansion, α is 5.3×10-6°C.

To evaluate the test device, three specimen sizes were chosen and they are described in the table below. L_{free} represents the unclamped portion of the specimen which is the value used to calculate the theoretical critical load using Euler's equation.

Table 1 Specimen dimensions and properties

Specimen	***E* (Gpa)**	**L_{Total}(m)**	**L_{free}(m)**	***a*(m)**	***b*(m)**	**I(m^4)**	**P_{cr} (kN)**
S 28	193	0.71	0.69	0.0254	0.00229	2.52861E-11	0.4092
S 30	193	0.76	0.74	0.0254	0.00229	2.52861E-11	0.3547
S 32	193	0.81	0.79	0.0254	0.00229	2.52861E-11	0.3104

Mechanical Model

The critical load P_{cr} of a specimen experimental is usually observed from a P vs δ curve. That would require a complete buckling response of the specimen and potentially deform the specimen plastically. The experiments intended to be performed on the specimens are restricted to the elastic region of the material. Therefore an accurate method capable of predicting the critical buckling of the specimen is needed.

Southwell's method is a widely used technique that provides a graphical method for nondestructive critical-load testing of columns as well as other structural components that may fail by buckling. It has already been used by Fisher in a combined axial and transverse loading (a typical loading for an airplane spar in test or flight. Southwell observed that for a lateral deflection δ_H under a given load $P < P_{cr}$ [13]

$$\delta_H = M\left(\frac{\delta_H}{P}\right) - k \tag{9}$$

Where $M = P_{cr}$ and k is a constant. Equation 9 is the equation of a straight line of slope P_{cr}. The Southwell plot is illustrated below. Derivation can be found in [12], [14].

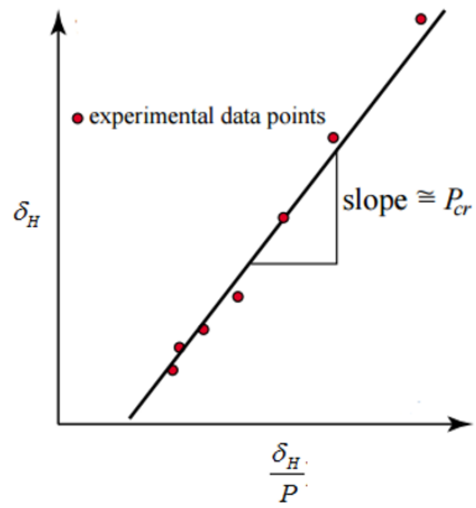

Figure 22 Southwell Plot

Chapter 4. Results

Mechanical

Combined

Chapter 5. Numerical Simulations

SOLIDWORKS is used to simulate the buckling experiment. Buckling analysis is tightly integrated with SOLIDWORKS CAD and allows the calculation of critical failure loads of slender structures under compression.

Figure 23 Software used for simulation

Specimen Model

First, a CAD model was generated for each specimen the exact dimension as shown below.

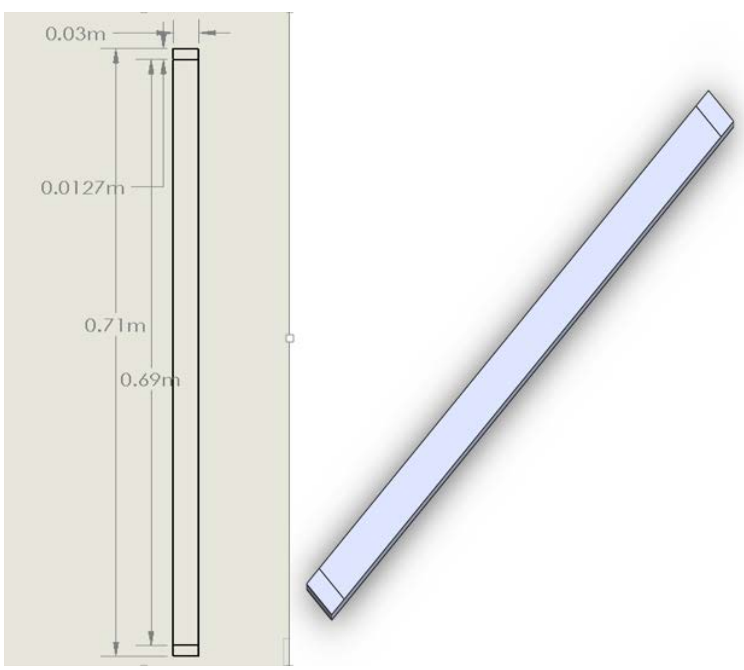

Figure 24 Specimen CAD and dimensions

The model was generated as close as possible to a real specimen. Surfaces were added at the extremities of the model to replicate the contact surfaces between the specimen and the clamps of the test device.

Finite Element Model

The next step in the finite element analysis was to set the boundary conditions. Two features were used to apply the boundary conditions to the model. A *fixed geometry* restraint was applied to the bottom of the specimen to set all the translational degrees of freedom to zero.

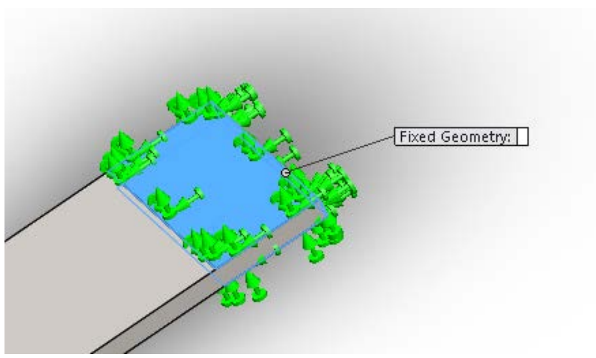

Figure 25 Fixed geometry feature

Then a Roller/Slider was applied to the top faces in contact with the clamps to only allow for vertical motion of the top extremity of the sample as a force is being applied to it. The extremities inside the Roller/Slider and fixed geometry constrains are not allowed to deflect or rotate (i.e. $\delta_H(0) = 0$, $\delta_H(L) = 0$).

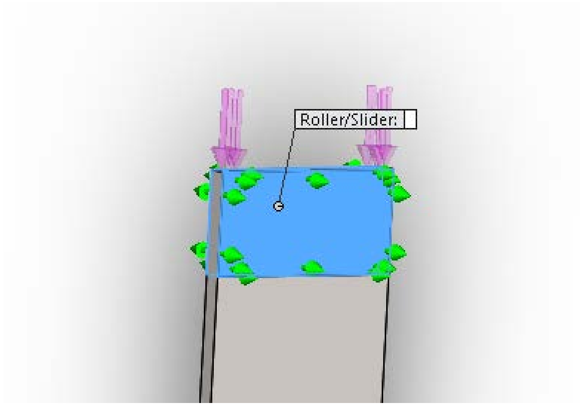

Figure 26 Roller/Sider feature

The load was applied normal to the bottom surface of the specimen for compression.

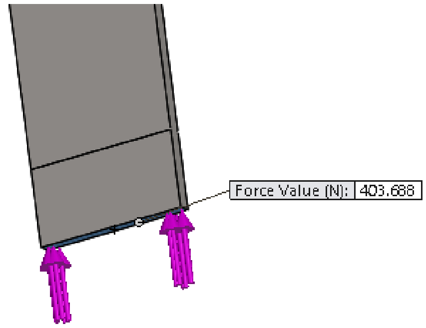

Figure 27 Load being applied to the specimen

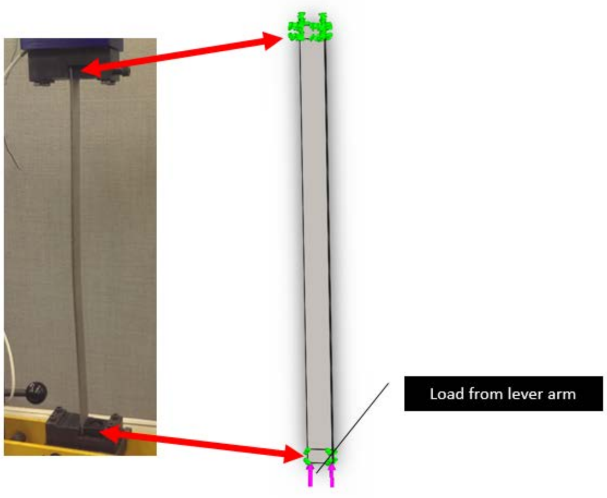

Figure 28 Final FEM model for buckling analysis

Results

The graphs below show the results of the buckling analysis of the specimens where the critical load and the maximum deformation are calculated. Those results are summarized in Table 2.

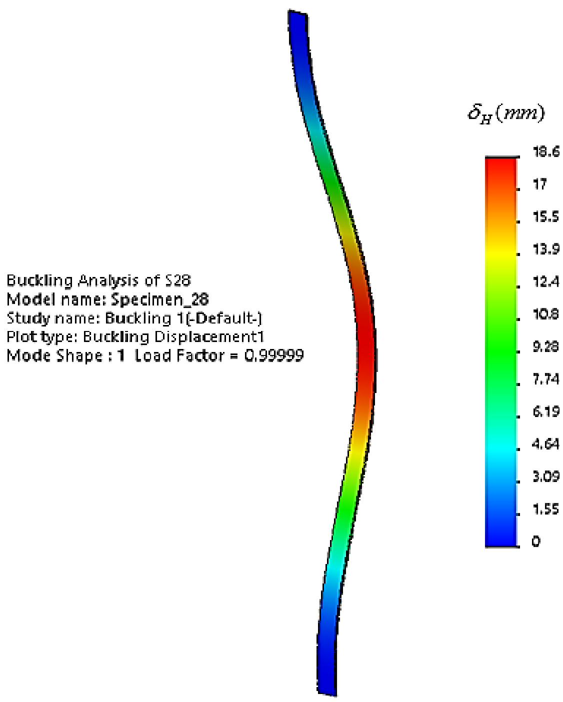

Figure 29 Buckling analysis of specimen S28

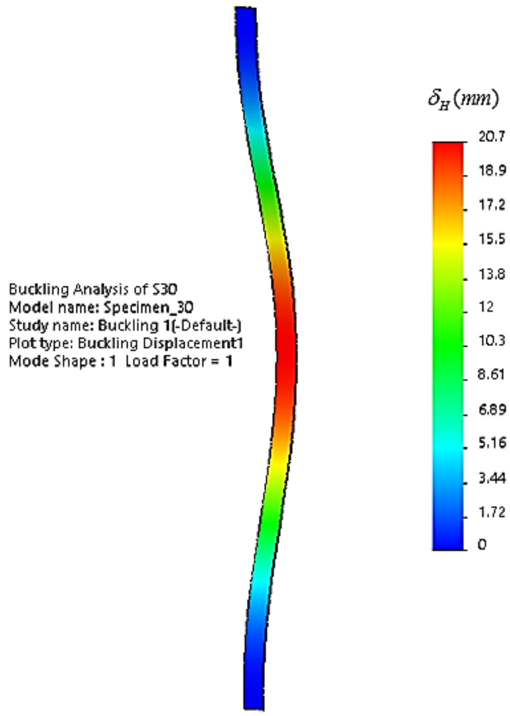

Figure 30 Buckling analysis of specimen S30

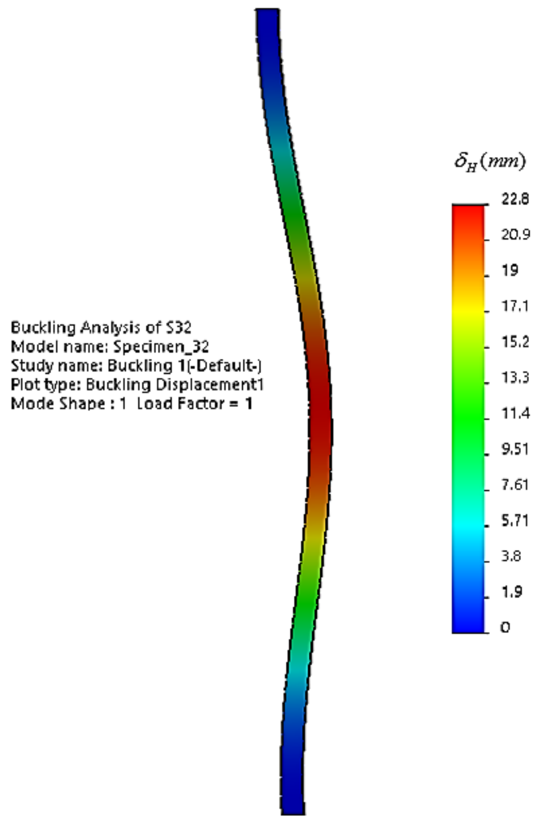

Figure 31 Buckling analysis of specimen S32

Table 2 Buckling analysis simulation

Specimen	**Pcr (kN)**	**$\delta_{H\ max}$(mm)**
S 28	0.4037	18.6
S 30	0.3502	20.7
S 32	0.3066	22.8

Chapter 6. Comparisons and Observations

Chapter 7. Conclusion

References

[1] Karasek M. L, Husehin Sehitoglu, and D. C. Slavik. "Deformation and Fatigue Damage in 1070 Steel Under Thermal Loading." *Low Cycle Fatigue* (1988): 184-205.

[2] Galambos, T. V. *Guide to Stability Design Criteria for Metal Structures, 4th ed.* New York: John Wiley, 1988.

[3] Wang C. M., Wang C. Y., Reddy J. N. *Exact Solution for Buckling of Structural Members*. Boca Raton: CRC Press LLC, 2005.

[4] Bazant, Zdenek P. *Stability of Structures*. New York: Oxford University Press, 1991.

[5] Hibbeler R., C. *Mechanics Of Materials*. Boston: Prentice Hall, 2011.

[6] Carpinteri A., Malvano R., Manuello A., Piana G. "Fundamental frequency evolution in slender beams." *Journal of Sound and Vibration* (2014): 2390–2403.

[7] Weiyong Wang, Venkatesh Kodur, Xingcai Yang, Guoqiang Li. "Experimental study on local buckling of axially compressed steel stub." *Thin-Walled Structures* (2014): 33–45.

[8] Abramovich, H. "Experimental Studies of Stiffened Composite Panels under Axial Compression, Toorsion and Combined Loading." Falzon B G & Aliabadi H M,. *Buckling and Postbuckling Structures*. London: Imperial College Press, 2008. 1-37.

[9] Ziółkowski A., Imiełowski S. "Buckling and Post-buckling Behavior of Prismatic Aluminum Columns Submitted to a Series of Compressive Loads." *Experimental Mechanics* (2011): 1335–1345.

[10] Wang, Y. C., and Moore, D. B. "‘Effect of thermal restraint on column behaviour in a frame." *4th Int. Symp. on Fire Safety Science, T. Kashiwagi* (1994): 1055 – 106

[11] Archer, Robert R, and Thomas J Lardner. *An Introduction to the Mechanics of Solids*. New York: McGraw-Hill, 1978. Print.

[12] Singer, J, Johann Arbocz, and T Weller. *Buckling Experiments*. Chichester: Wiley, 1998. Print.

[13] Fisher, H. R. 'An Extension of Southwell's Method of Analyzing Experimental Observations in Problems of Elastic Stability'. *Proceedings of the Royal Society A: Mathematical, Physical and Engineering Sciences* 144.853 (1934): 609-630. Web.

[14] Hoff, Nicholas J. *The Analysis Of Structures, Based On The Minimal Principles And The Principle Of Virtual Displacements*. New York: Wiley, 1956. Print.